Modeling of a Multiannular Photocatalytic Reactor for Perchloroethylene Degradation in Air

Gustavo E. Imoberdorf, Alberto E. Cassano, Orlando M. Alfano, and Horacio A. Irazoqui
INTEC, Instituto de Desarrollo Tecnológico para la Industria Química, Universidad Nacional del Litoral and CONICET, 3000 Santa Fe, Argentina

DOI 10.1002/aic.10771
Published online January 17, 2006 in Wiley InterScience (www.interscience.wiley.com).

The full modeling and simulation of a multiannular photocatalytic reactor requires a thorough physical analysis of all the concurrent phenomena determinant of its performance: momentum and mass transfer in the homogeneous, nonuniform, fluid phases; radiation transfer in the fluid phases and across the flow physical boundaries; and heterogeneous photocatalytic reaction kinetics. In a previous work, an expression of the intrinsic kinetics for the degradation of perchloroethylene (PCE) based on a plausible reaction mechanism was proposed and experimentally validated. In this work, this expression is used in the physical modeling and mathematical simulation of a multiannular, bench-scale reactor. The reactor shows good effectiveness for the PCE degradation in polluted moist air. A radiation field model was developed to predict the local superficial rate of photon absorption (LSRPA) at each point on the reactor catalytic walls, which is needed to evaluate the local reaction rate. A 2-D mass balance was developed taking into account the intrinsic kinetics, as well as mass-transfer rate processes and the LSRPA calculated with the radiation field model equations. Predicted conversions show good agreement with experimental results with a root mean square error $< 5.6\%$. © 2006 American Institute of Chemical Engineers *AIChE J,* 52: 1814–1823, 2006
Keywords: air pollution remediation, photocatalysis, tetrachloroethylene, multiannular photoreactor

Introduction

Photocatalytic reactors are effective in eliminating volatile organic compounds (VOCs) from air. They were tested for the elimination of several contaminants, including formaldehyde, toluene, acetone, ethanol, chloroform, carbon tetrachloride, and chlorinated ethylenes, among others.[1,2] These technologies acquire additional interest for industrial applications when incorporated into heating, ventilation, and air-conditioning systems to improve indoor air quality.

At industrial-scale perchloroethylene (PCE) is used as a solvent in dry cleaning and metal degreasing facilities as well as in plastic manufacturing, fumigation, and textile processing. PCE is noninflammable, chemically stable, and has excellent washing properties. However, this compound is toxic, carcinogenic, and extremely persistent in the environment.

Most of the scientific literature concerning the photocatalytic degradation of chlorinated ethylenes in the gas phase report studies based on trichloroethylene (TCE) as the model compound.[3-10] Few studies on tetrachloroethylene (or PCE) oxidation can be found in the scientific literature,[11,12] in which all of them use a reaction scheme similar to that of TCE.

The modeling of a multiannular photocatalytic reactor requires the resolution of the momentum and mass-transfer equations in the gas phase, the radiation transfer equation in the fluid phases and across the flow physical boundaries, and the heterogeneous photocatalytic reaction kinetics.[13,14] This physical analysis opens the way to make every reasonable simplifying assumption, leading to more manageable mathematical models that facilitate the interpretation of the re-

Correspondence concerning this article should be addressed to O. M. Alfano at alfano@intec.unl.edu.ar.

sults obtained, in most cases, by means of numerical computations.

Few photoreactor configuration models have been studied so far. Hall et al.[15] developed a theoretical model to predict the degradation of volatile organic compounds in a honeycomb monolith photoreactor. The model was based on equations of UV radiation propagation, transport of gaseous contaminants to the catalytic surface, and the heterogeneous photocatalytic reaction. For the reflection of radiation on physical walls, weighted contributions of both the diffuse and the specular reflection models were used. Intrinsic destruction rates measured in a flat-plate laboratory reactor were used to model the heterogeneous photocatalytic reaction. Nicolella and Rovatti[16] proposed a plug-flow model for a monolith channel irradiated by an external source. Photocatalytic and thermal reactions were found to occur at the same time. Operating conditions for the prevalence of each one of these mechanisms were identified. Hossain et al.[17] reported a three-dimensional (3-D) convection–diffusion–reaction mathematical model for a titanium-coated honeycomb monolith photoreactor. The expression of the reaction rate and the values of the kinetic parameters were previously determined using a flat-plate reactor. The kinetic expression used depends on the local UV light intensity and the local reactant concentration. The model is based on a rigorous description of the fluid velocity and concentration fields. The local mass-transfer rate is determined using local diffusive and convective fluxes rather than average mass-transfer coefficients. For the range of operating conditions used, good agreement between model predictions and experimental pilot-scale formaldehyde conversion measurements was obtained.

Changrani and Raupp[18] developed a two-dimensional (2-D) heterogeneous convection–reaction model for an annular photocatalytic reactor filled with reticular foam. Mass balances for individual species are coupled through the boundary condition at the fluid–solid interface, which includes the heterogeneous reaction rate as the source/sink term, modeled as a semiempirical Langmuir–Hinshelwood–Watson kinetics that includes adsorption constants for various species. The *local volumetric rate of photon adsorption* (LVRPA) term in the rate expression was computed using a 3-D polychromatic radiation–field model. Isopropanol was chosen as the model pollutant to validate the theoretical predictions. Wang and Ku[19] proposed a simplified model to describe the decomposition of benzene in a batch photoreactor with TiO_2-coated optical fibers. They adopted a bimolecular Langmuir–Hinshelwood kinetic model and a simplified UV light absorption model corresponding to that of a well-mixed reactor.

Monoliths operate with a low pressure drop and provide a reasonable surface area per unit reactor volume. Nonetheless, they show a poor radiation penetration: The light intensity at a 3–4 aspect ratio distance from the channel mouth falls to 1% of the incident light intensity.[20] In this work, a multiannular photoreactor was conceived and designed to preserve the advantages of the monolith configuration, while avoiding its shortcomings by improving the radiation usage. It consists of four borosilicate glass tubes (UV transparent) concentrically arranged, forming annular channels, where the polluted air flows. A black-light UV lamp, placed at the centerline of the photoreactor, is the source of near-UV radiation. The TiO_2 photocatalyst was deposited as a thin film on the borosilicate glass tubes by means of a sol–gel technique. A radiation model

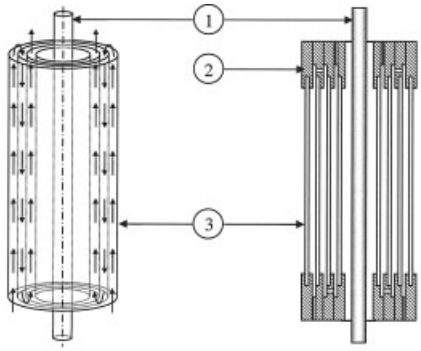

Figure 1. Geometry of the multiannular photocatalytic reactor.

(1) UV lamp, (2) distribution heads, (3) borosilicate glass tubes.

was developed to predict the *local superficial rate of photon absorption* (LSRPA) at each point on the reactor walls, needed to calculate the local reaction rate. The radiation field model includes a 3-D light source model with superficial emission[13,21] to simulate the lamp used in the bench-scale prototype. The model also accounts for the attenuation of the propagating light beams as they traverse the different media encountered in their way from the lamp to the TiO_2 films. A previously developed kinetic model, a mass-transfer model, and the radiation field model are assembled into a differential 2-D mass balance. A kinetic expression for the photocatalytic degradation of PCE contaminating an air stream was obtained from a previous work.[22,23] The experiments were carried out for different values of PCE feed concentrations, relative humidity, and irradiation levels in a coated-plate photoreactor operated under kinetic control regime, free of mass-transfer interference. The TiO_2 was deposited on a borosilicate glass plate as a thin film by means of a sol–gel technique. An expression of the intrinsic overall reaction rate was derived from a mechanism including the absorption of radiant energy on the catalytic surface as the primary step, followed by a detailed reaction sequence that involves $Cl^{\bullet}$ as an active intermediate species. The kinetic expression was validated against experimental results obtained from a flat-plate photoreactor operated as a differential one, and the kinetic parameters were determined by nonlinear regression from those results.

By the simultaneous numerical solution of the models before, it was possible to predict the behavior of the multiannular photoreactor.

Experimental

As sketched in Figure 1, the reactor consists of four concentric cylindrical, borosilicate glass tubes that are transparent to UV radiation in most of the useful wavelength range (from 300 to 420 nm). A tubular UV lamp (Philips TL 18W/08 F4T5/BLB) was placed at the central axis of the system. The reactor dimensions are shown in Table 1. Reactants and products flow through the annular spaces, entering the reactor by the external annular space and leaving it by the internal one. The two walls directly in contact with the gas flowing through each annulus are covered with a thin layer of TiO_2. The inner and the outer tubes are covered only on the side in contact with the contam-

Table 1. Reactor Dimensions and Characteristics

Description	Values
Lamp	$Z_L = 59$ cm; $R_L = 1.4$ cm; $P = 3.5$ W
Reactor	$Z_R = 48$ cm; $R_{R,int} = 1.48$ cm; $R_{R,ext} = 4.26$ cm
Annulus 1	$\chi_1 R_1 = 1.69$ cm; $R_1 = 2.31$ cm
Annulus 2	$\chi_2 R_2 = 2.51$ cm; $R_2 = 3.30$ cm
Annulus 3	$\chi_3 R_3 = 3.53$ cm; $R_3 = 3.94$ cm

inated air stream. Thin layers of TiO_2 were deposited using the sol–gel technique,[24] except for few modifications. A volume of 1660 cm^3 of triple-distilled water was mixed with 18 cm^3 of concentrated nitric acid (Anedra, 65%). A solution of titanium isopropoxide (140 cm^3, 97%, Aldrich) was then added to this mixture and peptized under stirring at 80°C for 10 h until a clear sol was obtained. Then, 0.01% of a surfactant was added to promote a uniform spreading of the TiO_2 on the carefully cleaned supporting tubes. These tubes were washed with isopropyl alcohol and triple-distilled water. The films were deposited by dip-coating of the tubes in the liquid mixture at a withdrawal speed of 3 cm min^{-1} at room temperature (25°C). The tubes were dried in an oven at 80°C and then calcined at 200°C for 6 h. A thorough characterization of this type of materials can be found in the published studies by Bischoff and Anderson,[25] Yamazaki et al.,[26] and Yun et al.[27]

As stated before, the purpose of this work is to test a physical and mathematical reactor model against experimental results obtained for a defined range of operating conditions. Total mineralization of contaminant PCE has been achieved with the reactor operating at full lamp radiation output. Although reassuring when considering future practical applications, these operating conditions are not useful for model-checking purposes because we cannot experimentally determine the limiting conditions under which the reactor outlet stream bears, at least, traces of PCE without incurring a large expenditure of reactants by using a very large flow rate. To get around this problem we chose to attenuate the radiation coming from the lamp. The radiation flux reaching the photoreactor was lowered by interposing specially constructed filters[28] between the lamp and the reactor inner wall. These filters were constructed on polyester films (0.1 mm thick), red-sensitive for recorders with He–Ne laser (HNm from AGFA Alliance Recording), by printing different tones of gray with the aid of software. The good optical and mechanical stabilities of these films were confirmed by exposing them to the radiation from the lamp for >15 h, with no measurable changes of their spectral transmittance.

The experimental setup is schematically shown in Figure 2. The photoreactor feed stream results from the mixture of an air stream with a water-saturated air stream and a PCE–air stream. Preestablished ratios between the mass flows of these streams enabled us to obtain a controlled operation, as well as the desired PCE concentration and humidity. The air used was of chromatographic quality (Air Liquide). The PCE–air mixture was prepared from chromatographic air and liquid PCE (Merck, p.a. quality). The water-saturated air stream was obtained by bubbling the air stream through a saturation flask containing distillated water at 20°C. The flow rates of the three streams were controlled with on-line mass-flow controllers (Matheson Corp.). The temperature and the humidity of the feed stream were measured with an on-line thermohygrometer (Oakton 35612-00) located just upstream from the sampling point in the reactor feed line.

Before starting each experimental run, the operating variables were fixed at the preestablished values and then the lamp was turned on. Samples were taken from the two sampling points not before 3 h of continuous operation to ensure a constant light intensity and a steady-state regime of the reaction system. The PCE concentrations in the inlet and outlet streams were determined by off-line gas chromatography (Hewlett Packard 5890; J&W1257032 column; FID detector). The outlet stream was also analyzed by gas chromatography–mass spectroscopy (GC-MS) techniques (Shimadzu QP-5000), for detecting any possible stable intermediate species and/or reaction by-products. Spectral radiation absorptions of the glass tubes, TiO_2 films, and filters were measured with a UV–Vis spectrophotometer (Varian Cary, 100 Bio) as a function of the wavelength, within the emission range of the lamp.

Physical and Mathematical Model

Radiation absorption field

The LSRPA was evaluated at each point on the TiO_2 films, taking into account the radiation incident from all feasible directions. Although the borosilicate glass tubes that support the TiO_2 catalyst have satisfactory UV transmission properties in the range 300–420 nm, this material attenuates the intensity of the UV radiation beams to some extent. The model of the radiation field makes allowance for this effect.

The local net radiation flux, corresponding to a given wavelength λ, is given by

$$q_\lambda(\mathbf{x}) = \mathbf{n}_G \cdot \mathbf{q}_\lambda = \int_\Omega I_\lambda(\mathbf{x}, \mathbf{\Omega})\mathbf{\Omega} \cdot \mathbf{n}_G d\Omega \qquad (1)$$

where $\mathbf{n}_G$ is the unit outwardly directed normal to the film surface and I_λ is the intensity of a beam carrying energy of wavelength λ in the direction $\mathbf{\Omega}$. The radiation field remains invariant under virtual rotations of the reactor about its centerline. Therefore, among other field properties, the local net radiation flux will depend only on the (r, z) pair of coordinates. Applying Eq. 1 to each point on the external surface of one of

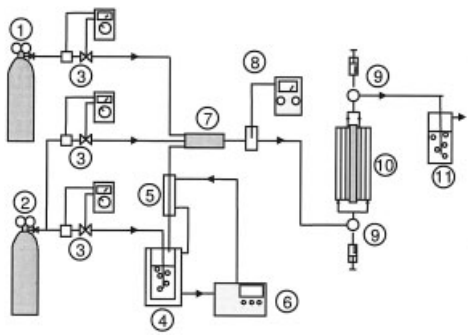

Figure 2. Flow sheet of the experimental device.

(1) PCE + air, (2) air, (3) mass flowmeter, (4) air humidifier, (5) heat exchanger, (6) thermostatic bath, (7) mixer, (8) thermohygrometer, (9) sampling device, (10) photoreactor, (11) gas scrubber.

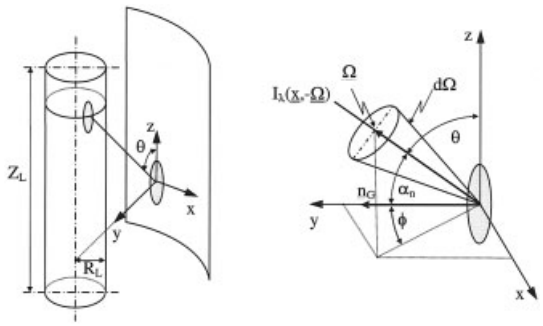

Figure 3. Coordinate system.

the very thin catalytic films, with the coordinate system adopted (Figure 3), we have

$$q_\lambda(r, z) = \int_\phi \int_\theta I_\lambda(r, z, \phi, \theta)\cos\phi \sin^2\theta d\theta d\phi \qquad (2)$$

To solve this equation we will use the *three-dimensional source with superficial emission* model[13,21] and the ray-tracing method. The lamp model relies on the following assumptions: (1) the lamp is a perfect cylinder, (2) the photon emitters are distributed uniformly on the lamp surface, (3) each point of the lamp surface emits isotropically, and (4) there are no changes in the direction or intensity of the rays when they leave the lamp surface. The radiation beams coming directly from the lamp, which are incident on a film differential area at a position (r, z), can have directions included only within the limits defined by the lamp contour, as seen from the point of incidence. This contour is the solution of the following set of equations:

$$\phi_{\max}(r) = \cos^{-1}\left(\frac{\sqrt{r^2 - R_L^2}}{r}\right) \qquad \phi_{\min}(r) = -\cos^{-1}\left(\frac{\sqrt{r^2 - R_L^2}}{r}\right) \qquad (3)$$

$$\theta_{\max}(r, z, \phi) = \tan^{-1}\left(\frac{r\cos\phi - \sqrt{R_L^2 - r^2\sin\phi^2}}{z}\right)$$
$$\theta_{\min}(r, z, \phi) = \tan^{-1}\left(\frac{r\cos\phi - \sqrt{R_L^2 - r^2\sin\phi^2}}{Z_L - z}\right) \qquad (4)$$

From the lamp model, the following boundary conditions result:

$$I_\lambda(r, z, \phi, \theta) = \begin{cases} 0 & (\phi, \theta) < (\phi_{\min,i}, \phi_{\min,i}) \\ I_{\lambda,L} = \dfrac{P_{\lambda,L}}{2\pi^2 R_L Z_L} & (\phi_{\min,i}, \theta_{\min,i}) < (\phi, \theta) < (\phi_{\max,i}, \theta_{\max,i}) \\ 0 & (\phi_{\max,i}, \theta_{\max,i}) < (\phi, \theta) \end{cases} \qquad (5)$$

where $P_{\lambda,L}$ is the spectral emission power of the lamp and R_L and Z_L are the radius and length of the lamp, respectively.

In the radiation field model, no participative medium has been considered other than the borosilicate tube walls and the catalytic films. This is so because air, PCE, and water vapor do not absorb radiation in the wavelength range of the lamp emission. Substitution of Eqs. 3 to 5 into Eq. 2 gives

$$q_\lambda(r, z) = \int_{\phi_{\min}(r)}^{\phi_{\max}(r)} \int_{\theta_{\min}(r,z,\phi)}^{\theta_{\max}(r,z,\phi)} I_{\lambda,L}\cos\phi \sin^2\theta d\theta d\phi \qquad (6)$$

At every position on the thin catalytic film, the LSRPA can be obtained from the local net fluxes resulting from all incident radiation beams coming from the lamp. This operation is schematically shown in Figure 4, where q_λ^i and q_λ^t are positive numbers:

$$e_\lambda^{a,s}(r, z) = q_\lambda^i(r, z) - q_\lambda^t(r, z) \qquad (7)$$

By replacing Eq. 6 in Eq. 7, and considering the attenuation effects produced by each participative medium in the path of the radiation beams, the final expression of the LSRPA at a given position on a thin catalytic film is

$$e^{a,s}(r, z) = \sum_{\lambda=300\text{nm}}^{420\text{nm}} \int_{\phi_{\min}(r)}^{\phi_{\max}(r)} \int_{\theta_{\min}(r,z,\phi)}^{\theta_{\max}(r,z,\phi)} I_{\lambda,L}\exp\left[-n_g(r)\frac{\kappa_{\lambda,g}e_g}{\cos\alpha_n} - n_f(r)\frac{\kappa_{\lambda,f}e_f}{\cos\alpha_n}\right] \times \left[1 - \exp\left(-\frac{\kappa_{\lambda,f}e_f}{\cos\alpha_n}\right)\right]\cos\phi \sin^2\theta d\theta d\phi \qquad (8)$$

where the integration limits ϕ and θ depend on both the geometry of the system and that of the lamp; $\kappa_{\lambda,f}$ and $\kappa_{\lambda,g}$ are the spectral absorption coefficients of the TiO_2 film and the glass tubes, respectively; e_f and e_g represent the thickness of the respective media; α_n is the angle between the ray trajectory and the film outwardly directed normal; and n_g and n_f are the number of times that a radiation beam has been attenuated by a glass tube wall or a TiO_2 film, respectively, before its incidence at the (r, z) position on the catalytic surface (Table 2). Values of $\kappa_{\lambda,g}e_g$ and $\kappa_{\lambda,f}e_f$ were determined from spectral transmittance measurements.

The mean value of the LSRPA on the reactor catalytic

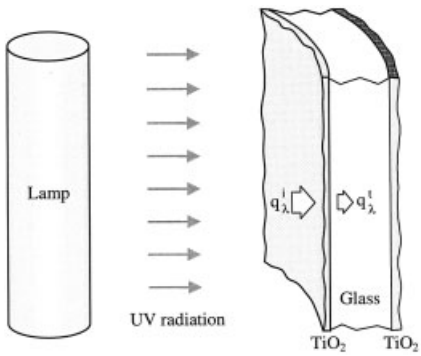

Figure 4. Radiation fluxes on the TiO_2 film.

Table 2. Numerical Values of $n_g(r)$ and $n_f(r)$

	$n_g(r)$	$n_f(r)$
$\chi_1 R_1$	1	0
R_1	1	1
$\chi_2 R_2$	2	2
R_2	2	3
$\chi_3 R_3$	3	4
R_3	3	5

surface is the *superficial rate of photon absorption* (SRPA), defined as follows:

$$\langle e^{a,s}\rangle_{A_R} = \frac{\int_{A_R} e^{a,s}(r, z)dA}{A_R} \tag{9}$$

Considering all possible contributions to the value of the SRPA, Eq. 9 may be written as

$$\langle e^{a,s}\rangle_{A_R} = \frac{\sum_{j=1}^{3}\int_{z=0}^{Z_R}[\chi_j R_j e^{a,s}(\chi_j R_j, z) + R_j e^{a,s}(R_j, z)]dz}{Z_R\sum_{j=1}^{3}(\chi_j R_j + R_j)} \tag{10}$$

where Z_R is the reactor length and $\chi_j R_j$ and R_j are the inner and outer radius of the jth duct of annular cross section with $j = 1$, 2, 3 when numbering starts from the inner one, respectively.

Kinetic model

In a previous work,[23] an expression of the intrinsic reaction rate was derived from the reaction scheme of Table 3. This mechanism is based on that proposed by Sanhueza et al.[29] for TCE degradation in the gas phase. Although there is no full agreement with respect to this mechanism, this reaction scheme was also used by many investigators.[5-10] Moreover, Yamazaki et al.[12] proposed a similar mechanism for the PCE degradation reaction.

The adopted reaction scheme relies on the assumption that the $Cl^{\bullet}$ radical attack on the PCE double bond plays an important role in the degradation process. More precisely, it is assumed that the PCE degradation reaction occurs through two parallel paths: (1) an elementary reaction involving the PCE attack by $OH^{\bullet}$, followed by a sequence of steps that leads to the generation of a $Cl^{\bullet}$ radical (steps from 3 to 6 in the mechanism of Table 3) and (2) a chain reaction initiated by the attack of $Cl^{\bullet}$ on the PCE, followed by the sequence composed of steps 7 to 14. This last sequence is able to regenerate $Cl^{\bullet}$ radicals through steps 11 and 14. Although in this scheme the main active species for PCE degradation is the $Cl^{\bullet}$ radicals, the attack of the $OH^{\bullet}$ radicals on PCE is a necessary step to generate the $Cl^{\bullet}$ radicals. Because of the very high reactivity of the $Cl^{\bullet}$ radical, it is possible to propose several termination reactions. To simplify the kinetic expression, in our model we have grouped them in a single reaction: $Cl^{\bullet} + M \rightarrow$ Products, where M may be water, other radicals, the reactor walls, or other surfaces.[30]

Assuming that: (1) the PCE elimination through the first step of the ($Cl^{\bullet}$) chain-propagation mechanism is much faster than that involving the direct hydroxyl attack[8,9]; (2) the micro-steady-state approximation (MSSA) may be applied to the net generation rates of free radicals ($OH^{\bullet}$, $Cl^{\bullet}$), "free" electrons (e^-), and holes (h^+)[31]; (3) the surface concentrations of adsorbed PCE and water can be obtained from a balance of active sites, taking into account that PCE and water compete for the same adsorption sites[21,32]; and (4) surface concentrations can be related to gas-phase concentrations by the adsorption equilibrium,[33] we obtain

$$r_{\mathrm{PCE}} = -\frac{k_1 k_2 k_7 K_{\mathrm{PCE}} K_{\mathrm{H_2O}} C_S^2 C_{\mathrm{O_2}} C_{\mathrm{PCE}} C_{\mathrm{H_2O}}}{2k_{15}k_{16}C_M(1 + K_{\mathrm{PCE}}C_{\mathrm{PCE}} + K_{\mathrm{H_2O}}C_{\mathrm{H_2O}})^2} \times\left(-1 + \sqrt{4k_{15}\frac{1 + K_{\mathrm{PCE}}C_{\mathrm{PCE}} + K_{\mathrm{H_2O}}C_{\mathrm{H_2O}}}{k_1 k_2 K_{\mathrm{H_2O}} C_S C_{\mathrm{O_2}} C_{\mathrm{H_2O}}}\bar{\Phi}e^{a,s} + 1}\right) \tag{11}$$

where K_{PCE} and $K_{\mathrm{H_2O}}$ are the adsorption constants of PCE and water on the TiO_2 catalyst film, respectively; $\bar{\Phi}$ is the wavelength averaged primary quantum yield; and [Sites] stands for the equilibrium surface concentration of sites available for adsorption.

For the same operating conditions, Imoberdorf et al.[23] found that Eq. 11 can be simplified to give

$$r_{\mathrm{PCE}} = -\frac{k_7 K_{\mathrm{PCE}} C_S \bar{\Phi}}{k_{16} C_M}\frac{C_{\mathrm{PCE}}}{1 + K_{\mathrm{H_2O}}C_{\mathrm{H_2O}}}e^{a,s} = -\alpha\frac{C_{\mathrm{PCE}}}{1 + K_{\mathrm{H_2O}}C_{\mathrm{H_2O}}}e^{a,s} \tag{12}$$

The parameters in the reaction rate expression were regressed from experimental data using the Levenberg–Marquardt method, the values of which were $\alpha = 1.54 \times 10^8$ (cm^3 $Einstein^{-1}$) and $K_{\mathrm{H_2O}} = 3.21 \times 10^{-4}$ (m^3 mg^{-1}).

Gas flow through the reactor concentric annular ducts

The Reynolds number for the gas flow through the jth duct is

$$\mathrm{Re}_j = \frac{4r_{h,j}G}{\mu} = \frac{2Q\rho}{\pi\mu R_j(1 + \chi_j)} \qquad (j = 1, 2, 3) \tag{13}$$

Table 3. Reaction Scheme

Initiation:	$TiO_2 \rightarrow TiO_2 + e^- + h^+$	r_g
	$h^+ + H_2O_{ads} \rightarrow OH\cdot + H^+$ $h^+ + HO^-_{ads} \rightarrow OH\cdot$	k_1
	$e^- + O_2 \rightarrow O_2^-\cdot$	k_2
($Cl^{\bullet}$) generation:	$C_2Cl_{4\ ads} + OH^{\bullet} \rightarrow C_2Cl_4OH^{\bullet}$	k_3
	$C_2Cl_4OH^{\bullet} + O_2 \rightarrow C_2Cl_4OHOO^{\bullet}$	k_4
	$2C_2Cl_4OHOO^{\bullet} \rightarrow 2C_2Cl_4OHO^{\bullet} + O_2$	k_5
	$C_2Cl_4OHO^{\bullet} \rightarrow C_2Cl_3OHO + Cl^{\bullet}$	k_6
Chain propagation:	$C_2Cl_{4\ ads} + Cl^{\bullet} \rightarrow C_2Cl_5^{\bullet}$	k_7
	$C_2Cl_5^{\bullet} + O_2 \rightarrow C_2Cl_5OO^{\bullet}$	k_8
	$2C_2Cl_5OO^{\bullet} \rightarrow 2C_2Cl_5O^{\bullet} + O_2$	k_9
	$C_2Cl_5O^{\bullet} \rightarrow CCl_2O + CCl_3^{\bullet}$	k_{10}
	$C_2Cl_5O^{\bullet} \rightarrow C_2Cl_4O + Cl^{\bullet}$	k_{11}
	$CCl_3^{\bullet} + O_2 \rightarrow CCl_3OO^{\bullet}$	k_{12}
	$2CCl_3OO^{\bullet} \rightarrow 2CCl_3O^{\bullet} + O_2$	k_{13}
	$CCl_3O^{\bullet} \rightarrow CCl_2O + Cl^{\bullet}$	k_{14}
Termination:	$e^- + h^+ \rightarrow$ heat	k_{15}
	$Cl^{\bullet} + M \rightarrow$ Products	k_{16}
Nonradical reaction:	$CCl_2O + H_2O \rightarrow CO_2 + 2HCl$	
Adsorptions equilibrium:	$C_2Cl_4 + \mathrm{Site} \leftrightarrow C_2Cl_{4\ ads}$	K_{PCE}
	$H_2O + \mathrm{Site} \leftrightarrow H_2O_{ads}$	$K_{\mathrm{H_2O}}$

where $r_{h,j}$ is the corresponding hydraulic radius, G is the mean mass velocity, Q is the gas volumetric flow rate, μ is the viscosity of the gas stream (for our purposes here, assimilated to air), and ρ is the gas density. Because of the reactor configuration, the largest value of the Reynolds number will occur in the innermost annulus, a value of about 25, far below the transition value from laminar to turbulent flow. On the basis of these results, we will make the following assumptions for the system operating at steady state:

(1) The gas flow through the annular ducts is a unidirectional, incompressible, and fully developed laminar flow along the entire useful reactor length, thus disregarding the relative importance of end effects.

(2) Newtonian fluid.

(3) Azimuthal symmetry.

(4) Constant physical properties.

The fully developed velocity profile for a laminar flow of a Newtonian fluid through the jth annular duct is

$$V_{z,j}(r) = (-1)^{j+1} \frac{2Q}{\pi R_j^2} \frac{\ln \chi_j}{[(1-\chi_j^4)\ln \chi_j + (1-\chi_j^2)^2]} \times \left[1 - \left(\frac{r}{R_j}\right)^2 - \frac{(1-\chi_j^2)}{\ln \chi_j} \ln\left(\frac{r}{R_j}\right)\right] \qquad (j = 1, 2, 3) \quad (14)$$

where the upward direction was chosen as the positive one.

Differential mass balance

The mass-transfer differential equation will be simplified on the basis of the following additional assumptions:

(5) Negligible contribution of the molecular diffusion mechanism to the total axial flow compared with the convective contribution. Then the axial flow is considered essentially convective, which means the remaining diffusive flux is important only along the radial direction.

(6) Because both the concentration of the more abundant species in the flowing gas mixture and its temperature are constants inside the reactor, the diffusivities of the species in the gas mixture are considered constant. Although always dilute, the only species that changes its concentration along the reactor in measurable percentages is PCE. Therefore, the radial diffusion can be considered as that of PCE in a more concentrated gas pseudocomponent, that is, air. This will be the governing mass-transfer mechanism of PCE from the bulk of the gas stream to the catalytic boundaries and of the reaction products in the opposite direction.

(7) Chemical reactions take place only on the photocatalytic film deposited on the annuli walls in contact with the flowing contaminated air stream or in its immediate vicinity. True homogeneous photochemical reactions are considered completely absent.

With assumptions (1) to (7), the differential mass-transfer equation can be written as

$$\frac{\partial C_{\mathrm{PCE}}(r,z)}{\partial z} V_{z,j}(r) = \frac{D^0_{\mathrm{PCE-Air}}}{r} \frac{\partial}{\partial r}\left[r \frac{\partial C_{\mathrm{PCE}}(r,z)}{\partial r}\right] \qquad (0 < z < Z_R;\ \chi_j R_j < r < R_j;\ j = 1, 2, 3) \quad (15)$$

with the boundary conditions

$$D^0_{\mathrm{PCE-Air}} \left.\frac{\partial C_{\mathrm{PCE}}(r,z)}{\partial r}\right|_{r=R_j} = r_{\mathrm{PCE}}[C_{\mathrm{PCE}}(R_j, z), C_{\mathrm{H_2O}}, e^{a,s}(R_j, z)] \qquad (0 < z < Z_R;\ j = 1, 2, 3) \quad (16)$$

$$D^0_{\mathrm{PCE-Air}} \left.\frac{\partial C_{\mathrm{PCE}}(r,z)}{\partial r}\right|_{r=\chi_j R_j} = -r_{\mathrm{PCE}}[C_{\mathrm{PCE}}(\chi_j R_j, z), C_{\mathrm{H_2O}}, e^{a,s}(\chi_j R_j, z)] \qquad (0 < z < Z_R;\ j = 1, 2, 3) \quad (17)$$

$$C_{\mathrm{PCE}}(r,z)|_{z=0} = C^0_{\mathrm{PCE}} \qquad (\chi_3 R_3 < r < R_3) \quad (18)$$

$$C_{\mathrm{PCE}}(r,z)|_{z=Z_R} = \frac{\int_{\chi_3 R_3}^{R_3} C_{\mathrm{PCE}}(r, Z_R) V_{z,3}(r) r dr}{\int_{\chi_3 R_3}^{R_3} V_{z,3}(r) r dr} \qquad (\chi_2 R_2 < r < R_2) \quad (19)$$

$$C_{\mathrm{PCE}}(r,z)|_{z=0} = \frac{\int_{\chi_2 R_2}^{R_2} C_{\mathrm{PCE}}(r, 0) V_{z,2}(r) r dr}{\int_{\chi_2 R_2}^{R_2} V_{z,2}(r) r dr} \qquad (\chi_1 R_1 < r < R_1) \quad (20)$$

where C_{PCE} is the PCE concentration, $D^0_{\mathrm{PCE-Air}}$ is the diffusion coefficient of PCE in air ($D^0_{\mathrm{PCE-Air}} = 0.072\ \mathrm{cm^2\ s^{-1}}$), and r_{PCE} is the superficial reaction rate.

The PCE conversion at the reactor outlet is computed as follows:

$$X_{\mathrm{PCE}} = \left[1 - \frac{\int_{\chi_1 R_1}^{R_1} C_{\mathrm{PCE}}(r, Z_R) V_{z,1}(r) r dr}{C^0_{\mathrm{PCE}} \int_{\chi_1 R_1}^{R_1} V_{z,1}(r) r dr}\right] \times 100 \quad (21)$$

Results

Numerical resolution of the mathematical model

The mathematical model was solved with an ad hoc developed FORTRAN program, based on the solution algorithm schematically shown in Figure 5. The operating conditions are shown in Table 4. The expression of the LSRPA was numerically computed at every point on each of the catalytic surfaces. This radiation variable depends on the physical characteristics and optical properties of different reactor components and parts, such as:

(1) the lamp radius and length, as well as on its emission power and the spectral distribution of the emitted radiation

(2) the spectral volumetric absorption of the borosilicate glass walls, as well as that of the TiO_2 films and of the neutral filter.

Nonetheless, the LSRPA does not depend on the PCE concentration because PCE does not absorb UV radiation in the useful wavelength range. For this reason the photon balance equation is not coupled with the mass-transfer equation and, therefore, it can be conveniently solved as a first step in the computational scheme.

The numerical results of LSRPA are shown in Figure 6. From these results, two conclusions can be drawn: (1) end

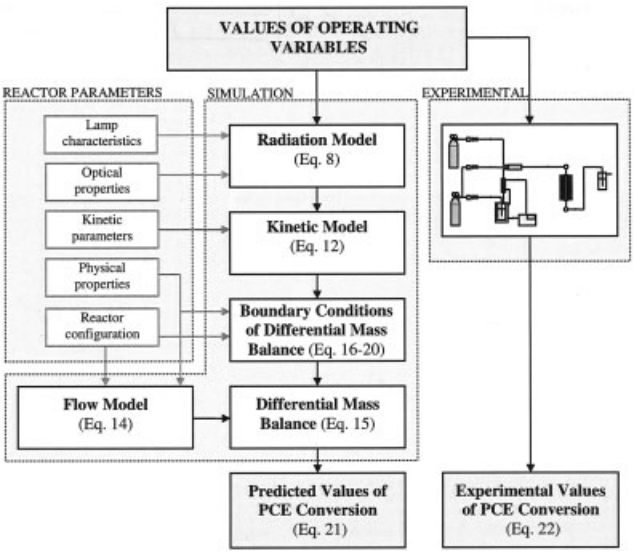

Figure 5. Algorithm used for numerical solution of the mathematical model.

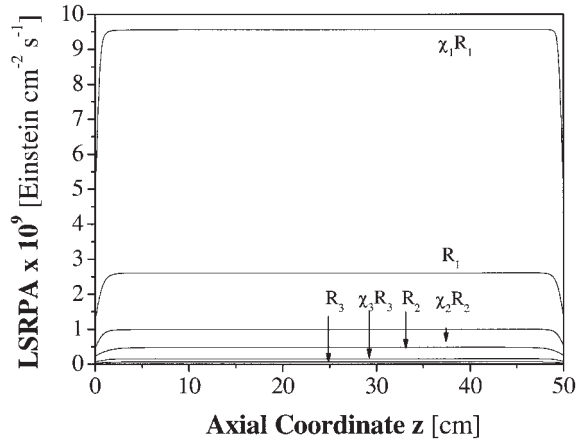

Figure 6. Numerical values of LSRPA on the TiO_2 films, without neutral filters.

effects on the LSRPA prediction are almost negligible and (2) the attenuation of radiation across each catalytic film is of primary importance.

The resulting LSRPA values are needed to compute the PCE reaction rate (Eq. 12) at each point on the catalytic surface. Because the PCE concentration was kept at very low levels in all the experimental runs (that is, <50 mg m^{-3}), the volumetric flow rate in the annular sections is, for all practical purposes, independent of the reaction rate. Therefore, the velocity profile could be directly computed from Eq. 14. The differential mass-transfer equation (Eq. 15), with the boundary conditions (Eqs. 16–20), was numerically solved using a method of finite differences. Finally, the PCE conversion was calculated from the discrete PCE profile at the reactor output stream (Eq. 21).

Experimental validation of the mathematical model

Preliminary experimental runs were performed at full lamp power output, without filtering. The experimental PCE conversion was evaluated by

$$X_{\mathrm{PCE}} = \frac{C^{in}_{\mathrm{PCE}} - C^{out}_{\mathrm{PCE}}}{C^{in}_{\mathrm{PCE}}} \times 100 \qquad (22)$$

No degradation of PCE was detected in the absence of either the TiO_2 photocatalyst or UV irradiation. Under the experimental operation conditions reported in Table 4, no stable intermediate species and/or reaction by-products were detected by GC-MS. The compounds present in the photoreactor outlet streams were identified as PCE, H_2O, CO_2, and HCl. We can thus assume that the PCE reacts to form CO_2 and HCl without the generation of stable intermediate species; that is, the global reaction is

$$\mathrm{PCE} + 2\mathrm{H_2O} \rightarrow 2\mathrm{CO_2} + 4\mathrm{HCl}$$

Although some degree of photocatalytic deactivation is observed in the long term, it has always been below detectable levels during the time elapsed along the complete set of runs of the experimental program. Important aspects such as photocatalytic deactivation are beyond the scope of the manuscript. Nevertheless, this problem has been studied by Larson and Falconer[34] and Lim and Kim,[35] among others.

The maximum affordable flow rate compatible with reasonable chromatographic quality air expenditure was 30 cm^3 s^{-1}. With that mass flow and with 48% relative humidity, the PCE outlet conversion predicted by the mathematical model was 99.93%. Meanwhile, the experimental PCE conversion was practically 100%, as can be concluded from the fact that no traces of PCE were detected by GC. These results indicate a good efficiency of the photoreactor performance, but of little (if any) use to test the reactor model. The overall reaction quantum efficiency (defined as the ratio of the number of molecules of PCE reacted to the number of photons absorbed by the catalyst films) depends on operating variables such as the PCE feed concentration and conversion, gas flow rate, irradiation level, relative air humidity, and mass-transfer limitations. Under the operative conditions used in this work, the values of the overall reaction quantum efficiency were $\leq$2.5%.

To obtain lower PCE conversions, useful for the experimental validation of the reactor model, different operating conditions were chosen. Because increasing the flow rate was an impractical option, the PCE conversion was decreased by depleting the intensity at any point of the radiation field using a neutral filter.

Although the radiation was substantially reduced, for the adopted range of flow rates the conversion values achieved were both important and useful for model-validating purposes.

Table 4. Experimental Operating Conditions

Operating Conditions	Value
Feed flow rate	2–30 cm^3 s^{-1}
Temperature	20°C
Pressure	1 atm
Inlet PCE concentration	50 mg m^{-3}
Relative humidity	10–90%
Reactive surface area	5205 cm^2
Irradiation level	1.0×10^{-11}–1.6×10^{-9} Einstein cm^{-2} s^{-1}

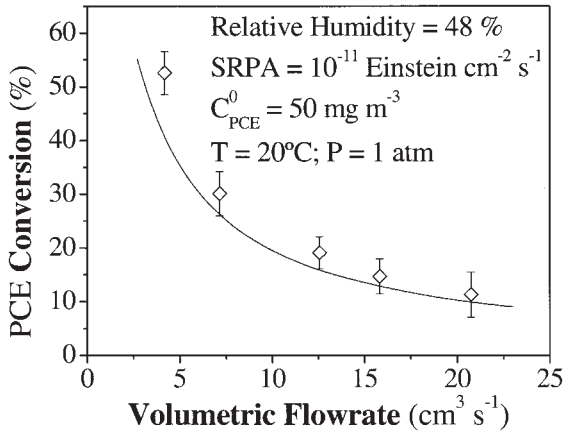

Figure 7. PCE conversion for different flow rates.

(◇) Experimental values, (—) model predictions.

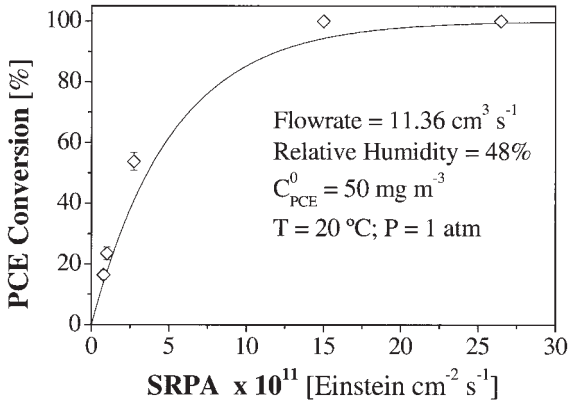

Figure 9. PCE conversion for different values of the SRPA.

(◇) Experimental values, (—) model predictions.

Figure 7 shows the model-predicted and the experimental PCE conversions as a function of volumetric flow rates, for relative humidity of 48% and SRPA equal to 1.0×10^{-11} Einstein cm^{-2} s^{-1}. It can be noted that the PCE outlet conversion decreases when the volumetric flow rate is increased. For example, PCE experimental conversions are 52.6 and 10.0% for volumetric flow rates of 4.2 and 21.8 cm^3 s^{-1}, respectively. Also notice that the maximum absolute deviation is no larger than 12.5% for $Q = 4.2$ cm^3 s^{-1}.

Figure 8 shows experimental and model PCE conversions as a function of the relative humidity. Constant values of the volumetric flow rate (12.5 cm^3 s^{-1}) and the SRPA (1.0×10^{-11} Einstein cm^{-2} s^{-1}) were used. Changing the relative humidity from 11.0 to 89.0%, the PCE outlet conversion decreases from 32.6 to 10.1%. As was suggested by Wang et al.[5] and Amama et al.,[9] this is the result of a competitive adsorption of water vapor and organic compound molecules for the active sites on the TiO_2 surface. An additional reason for the reaction inhibition was postulated by Amama et al.,[9] who proposed that the water vapor molecules suppress the chain reaction propagated by the chlorine atoms.

Total radiation flux at any point in the reactor was changed using different neutral filters and, consequently, the SRPA value. In Figure 9, the predicted effect of these changes on the PCE conversion is compared against experimental results. These runs were performed at a constant flow rate (11.36 cm^3 s^{-1}) and relative humidity (48%). It should be noted that, for values of SRPA $> 1.5 \times 10^{-10}$ Einstein cm^{-2} s^{-1}, the outlet PCE concentration is lower than the detection limit of the GC method used. Consequently, under these operating conditions, the PCE conversion is nearly 100%. For these experimental runs, the maximum absolute deviation is not >12.9%.

These results indicate that the simulation model is capable of predicting the experimental PCE outlet conversions with a high level of confidence. Considering the whole set of operating conditions used in this work, a root mean square error < 5.6% was obtained.

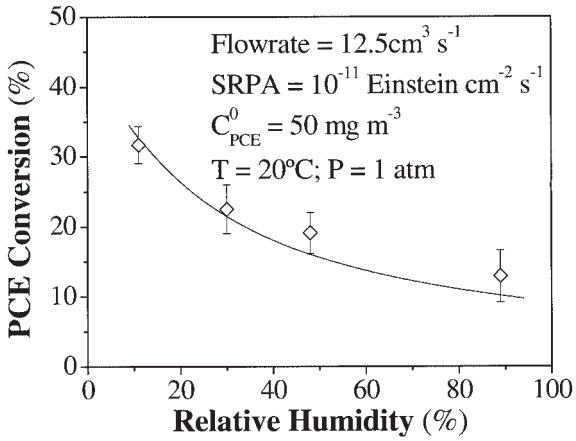

Figure 8. PCE conversion for different relative humidity values.

(◇) Experimental values, (—) model predictions.

Conclusions

A multiannular photocatalytic reactor was conceived and designed that shows good effectiveness for perchloroethylene (PCE) removal from contaminated air streams, without formation of stable intermediate species or by-products. This reactor configuration shares with monoliths their operating advantages (low pressure drop and good catalytic surface area per unit reactor volume), while showing a much better radiation distribution. The radiation distribution could be changed with the purpose of improving the reactor quantum efficiency by adopting a different TiO_2 film thickness for each concentric tube, thus opening the way for the search of an optimal design. An additional advantage of the annular photoreactors is that this reactor geometry is perhaps the simplest and most efficient configuration. Because most of the photons emitted by the radiation source arrive at the inner reactor walls, this reactor configuration has the highest reactor radiation incidence yield.

A physical and mathematical model for the multiannular concentric photoreactor was developed. It includes the kinetic model for PCE elimination from contaminated air presented in a previous work, as well as a radiation model and a mass-transfer model. The local superficial rate of photon absorption (LSRPA) at each point on the catalytic films was evaluated from a radiation model that does not make use of any experimentally adjusted parameters. Predicted PCE conversions

show satisfactory agreement when compared with experimental results with a root mean square error $< 5.6\%$.

The mathematical and computational model developed in this work can be used in the simulation and design modes as an unavoidable step toward the optimization and scale-up of photocatalytic reactors for abatement of air pollution.

Acknowledgments

The authors are grateful to Universidad Nacional del Litoral (UNL), Consejo Nacional de Investigaciones Científicas y Técnicas (CONICET), and Agencia Nacional de Promoción Científica y Tecnológica (ANPCyT) for financial support. Thanks are also given to Eng. Gerardo Rintoul for his participation in some parts of the experimental work.

Notation

A_R = photocatalytic surface area of the reactor, cm^2
C = mass concentration, mg m^{-3}
D^0 = molecular diffusivity, $cm^2\ s^{-1}$
e = thickness, cm
$e^{a,s}$ = local superficial rate of photon absorption, Einstein $s^{-1}\ cm^{-2}$
G = mean mass velocity, g $cm^{-2}\ s^{-1}$
I = specific radiation intensity, Einstein $s^{-1}\ cm^{-2}\ sr^{-1}$
K = equilibrium constant, $m^3\ mg^{-1}$
k_i = kinetic constant of the i reaction; units depend on the reaction step
$\mathbf{n}_G$ = unit outwardly directed normal to the catalytic film, dimensionless
P = emission power, W
Q = volumetric flow rate, $cm^3\ s^{-1}$
q = local net radiation flux, Einstein $s^{-1}\ cm^{-2}$
r = reaction rate, mol $cm^{-2}\ s^{-1}$; also radius, cm
r_h = hydraulic radius, cm
R = annulus radius, cm
R_L = lamp radius, cm
Re = Reynolds number, dimensionless
V_z = axial velocity, cm s^{-1}
$\mathbf{x}$ = position vector, cm
X = conversion, dimensionless
x = rectangular coordinate, cm
y = rectangular coordinate, cm
z = rectangular or cylindrical coordinate, cm

Greek letters

α = kinetic parameter, m^3 Einstein^{-1}
α_n = angle between the ray trajectory and the film outwardly directed normal, rad
ϕ = spherical coordinate, rad
Φ = primary quantum yield, mol Einstein^{-1}
κ = volumetric absorption coefficient, cm^{-1}
λ = wavelength, nm
θ = spherical coordinate, rad
Ω = solid angle, sr
μ = viscosity, g $cm^{-1}\ s^{-1}$
ρ = density, g cm^{-3}
χ = internal/external radius ratio, dimensionless

Subscripts

λ = denotes wavelength
A_R = reaction area of the photocatalytic plate
f = relative to the TiO_2 film
g = relative to the electron-hole generation step; also relative to glass
L = relative to the UV lamp
M = relative to water, reactor walls or other surfaces
max = relative to the maximum limit value
min = relative to the minimum limit value
n = normal to the reaction area of the photocatalytic surface
PCE = relative to perchloroethylene
R = relative to reactor
H_2O = relative to water

Superscripts

i = related to the incident radiation flux
in = relative to the inlet stream of the reactor
out = relative to the outlet stream of the reactor
t = related to the transmitted radiation flux

Special symbols

$\bar{\cdot}$ = averaged value over the wavelength interval
$\langle \cdot \rangle$ = means average value over a defined space

Literature Cited

1. Hoffman MR, Martin ST, Choi W, Bahnemann DW. Environmental applications of semiconductor photocatalysis. *Chem Rev.* 1995;95:69-96.
2. Blake DM. *Bibliography of Work on the Heterogeneous Photocatalytic Removal of Hazardous Compounds from Water and Air*. Golden, CO: National Renewable Energy Laboratory; 2001.
3. Dibble LA, Raupp GB. Kinetics of the gas–solid heterogeneous photocatalytic oxidation of trichloroethylene by near UV illuminated titanium dioxide. *Catal Lett.* 1990;4:345-354.
4. Hung CH, Mariñas BJ. Role of water in the photocatalytic degradation of trichloroethylene vapor on TiO_2 films. *Environ Sci Technol.* 1997; 31:1440-1445.
5. Wang KH, Tsai HH, Hsieh YH. The kinetics of photocatalytic degradation of trichloroethylene in gas phase over TiO_2 supported on glass bead. *Appl Catal B: Environ.* 1998;17:313-320.
6. Kim JS, Itoh K, Murabayashi M, Kim BA. Pretreatment of the photocatalyst and the photocatalytic degradation of trichloroethylene in the gas-phase. *Chemosphere.* 1999;38:2969-2978.
7. Li GH, An WZ. A proposed mechanism of photocatalytic oxidation of trichloroethylene in gas phase. *Chin Chem Lett.* 2000;11:31-34.
8. Zhao L, Ozaki S, Itoh K, Murabayashi M. Self-catalytic behavior in gas-phase photocatalytic oxidation of trichloroethylene using TiO_2. *Electrochemistry.* 2002;70:8-12.
9. Amama PB, Itoh K, Murabayashi M. Photocatalytic oxidation of trichloroethylene in humidified atmosphere. *J Mol Catal A: Chem.* 2001;176:165-172.
10. Wang KH, Jehng JM, Hsieh YH, Chang CY. The reaction pathway for the heterogeneous photocatalysis of trichloroethylene in gas phase. *J Hazard Mater.* 2002;B90:63-75.
11. Yamazaki S, Tsukamoto H, Araki K, Tanimura T, Tejedor-Tejedor I, Anderson MA. Photocatalytic degradation of gaseous tetrachloroethylene on porous TiO_2 pellets. *Appl Catal B: Environ.* 2001;33:109-117.
12. Yamazaki S, Araki K. Photocatalytic degradation of tri- and tetrachloroethylene on porous TiO_2 pellets. *Electrochemistry.* 2002;70:412-415.
13. Cassano AE, Martín CA, Brandi RJ, Alfano OM. Photoreactor analysis and design: Fundamentals and applications. *Ind Eng Chem Res.* 1995; 34:2155-2201.
14. Cassano AE, Alfano OM. Reaction engineering of suspended solid heterogeneous photocatalytic reactors. *Catal Today.* 2000;58:167-197.
15. Hall RJ, Bendfeldt P, Obee TN, Sangiovanni JJ. Computational and experimental studies of UV/titania photocatalytic oxidation of VOCs in honeycomb monoliths. *J Adv Oxid Technol.* 1998;3:243-252.
16. Nicolella C, Rovatti M. Mathematical modeling of monolith reactors for photocatalytic oxidation of air contaminants. *Chem Eng J.* 1998; 69:119-126.
17. Hossain MM, Raupp GR, Hay SO, Obee TN. Three-dimensional developing flow model for photocatalytic monolith reactors. *AIChE J.* 1999;45:1309-1321.
18. Changrani RG, Raupp GB. Two-dimensional heterogeneous model for a reticulated-foam photocatalytic reactor. *AIChE J.* 2000;46:829-842.
19. Wang W, Ku Y. Photocatalytic degradation of gaseous benzene in air streams by using an optical fiber photoreactor. *J Photochem Photobiol A: Chem.* 2003;159:47-59.
20. Hossain MM, Raupp GB. Polychromatic radiation field model for a

honeycomb monolith photocatalytic reactor. *Chem Eng Sci.* 1999;54: 3027-3034.
21. Stramigioli C, Santarelli F, Foraboschi FP. Photosensitized reactions in an annular continuous photoreactor. *Appl Sci Res.* 1977;33:23-44.
22. Imoberdorf G, Irazoqui H, Alfano O, Cassano A. Air pollution: Kinetics of the photocatalytic degradation of perchloroethylene in a coated plate reactor. In: Ollis DF, Al-Ekabi H, eds. *Photocatalytic and Advanced Oxidation Processes for Treatment of Air, Water, Soil and Surfaces*. Ontario, Canada: Redox Technologies, Inc.; 2005.
23. Imoberdorf GE, Irazoqui HA, Cassano AE, Alfano OM. Photocatalytic degradation of tetrachloroethylene in gas phase on TiO_2 films: A kinetic study. *Ind Chem Eng Res.* 2005;44:6075-6085.
24. Yamazaki-Nishida S, Nagano KJ, Phillips LA, Cervera-March S, Anderson MA. Photocatalytic degradation of trichloroethylene in the gas phase using TiO_2 pellets. *J Photochem Photobiol A: Chem.* 1993; 70:95-99.
25. Bischoff BL, Anderson MA. Peptization process in the sol–gel preparation of porous anatase (TiO_2). *Chem Mater.* 1995;7:1772-1778.
26. Yamazaki S, Fujinaga N, Araki K. Effect of sulfate ions for sol–gel synthesis of titania photocatalyst. *Appl Catal A: Gen.* 2001;210:97-102.
27. Yun YJ, Chung JS, Kim S, Hahn SH, Kim EJ. Low-temperature coating of sol–gel anatase thin films. *Mater Lett.* 2004;58:3703-3706.
28. Esterkin CR, Negro AC, Alfano OM, Cassano AE. Air pollution remediation. A fixed bed photocatalytic reactor made of glass fiber coated with TiO_2. *AIChE J.* 2005;51:2298-2310.
29. Sanhueza E, Hisatsune IC, Heiklen J. Oxidation of haloethylenes. *Chem Rev.* 1976;76:801-826.
30. Sauer ML, Hale MA, Ollis DF. Heterogeneous photocatalytic oxidation of dilute toluene–chlorocarbon mixtures in air. *J Photochem Photobiol A: Chem.* 1995;88:169-178.
31. Turchi CS, Ollis DF. Photocalytic degradation of organic water contaminants: Mechanisms involving hydroxyl radical attack. *J Catal.* 1990;122:178-192.
32. Hegedüs M, Dombi A. Gas-phase heterogeneous photocatalytic oxidation of chlorinated ethenes over titanium dioxide: Perchloroethene. *Appl Catal B: Environ.* 2004;53:141-151.
33. Zhao J, Yang X. Photocatalytic oxidation for indoor air purification: A literature review. *Build Environ.* 2003;38:645-654.
34. Larson SA, Falconer JL. Characterization of TiO_2 photocatalysts used in trichloroethene oxidation. *Appl Catal B: Environ.* 1994;4:325-342.
35. Lim TH, Kim SD. Trichloroethylene degradation by photocatalysis in annular flow and annulus fluidized bed photoreactors. *Chemosphere.* 2004;54:305-312.

Manuscript received July 30, 2005, and revision received Dec. 3, 2005.